MUSTA Schemes for Systems of Conservation Laws

E. F. Toro

Laboratory of Applied Mathematics
Faculty of Engineering, University of Trento
Trento, Italy
E-mail: toro@ing.unitn.it
Website: http://www.ing.unitn.it/toro

V. A. Titarev

Department of Mathematics
Faculty of Science, University of Trento
Trento, Italy
E-mail: titarev@science.unitn.it
Website: http://www.science.unitn.it/ titarev

Abstract. We present MUSTA-type upwind numerical fluxes that avoid the solution of the Riemann problem in the conventional manner. The upwinding of the present schemes comes instead, from a newly proposed numerical flux and the predictor-corrector procedure first reported in [23]. The proposed fluxes can be used as the building block for finite volume and discontinuous Galerkin finite element methods to solve hyperbolic conservations laws. Monotonicity, accuracy and stability properties of the schemes are established. Numerical implementations of the MUSTA schemes for the Euler equations for ideal gases, covolume gases and compressible liquids, in one, two and three space dimensions, are reported. The results demonstrate that the proposed schemes are comparable to those using *complete* Riemann solvers and superior to those using *incomplete* Riemann solvers. Our schemes however, have the added advantage of simplicity and generality, requiring only the vector of conserved variables, the vector of fluxes normal to the volume/element interface and appropriate closure conditions, such as equations of state. In this paper we also report on extensions of the MUSTA fluxes to higher order of accuracy via the TVD and WENO approaches for non-linear systems in one, two and three space dimensions.

Key words: Hyperbolic conservation laws; upwind methods, MUSTA fluxes, compressible materials, TVD methods, WENO methods, 3D non-linear systems.

1 Introduction

Numerical methods for solving non-linear systems of hyperbolic conservation laws via finite volume methods or discontinuous Galerkin finite element methods require, as the building block, a monotone numerical flux. The choice of the building block has a profound influence on the properties of the resulting schemes. There are essentially two approaches for providing a monotone numerical flux, the simplest of which utilizes a symmetric stencil and does not explicitly make use of wave propagation information, giving rise to *centred* or *symmetric* schemes [12], [8], [26], [28], [13], [1]. A more refined approach utilizes wave propagation information contained in the differential equations. This is done through the exact or approximate solution

of the Riemann problem, giving rise to *upwind* methods [3], [7], [16], [30], [18], [25]. For up-to-date background on these methods see, for example, [6], [11], [27].

Within the class of existing monotone first-order fluxes, the first-order upwind scheme of Godunov is the best, it has the smallest local truncation error. However, the superior accuracy of established upwind methods comes at a cost, one must solve exactly or approximately, the Riemann problem. Conventional Riemann solvers are usually complex and are not available for many hyperbolic systems of practical interest, such as for models for compressible multi-phase flows. It is thus desirable to construct a numerical flux that emulates the best flux available (upwind) with the simplicity and generality of symmetric schemes.

In this paper we build upon a newly proposed flux and the MUSTA approach [23] to construct schemes that have the simplicity and generality of symmetric schemes and the accuracy of upwind schemes. First we present a new flux that is a particular average of symmetric fluxes and which reproduces Godunov's upwind scheme for the model hyperbolic equation. For non-linear systems it is found that this flux gives superior results to those of the whole family of *incomplete* Riemann solvers that do not explicitly account for linearly degenerate fields, such as the HLL Riemann solver [9] and flux vector splitting schemes. Then we incorporate this flux into the MUSTA multi-staging approach, as predictor and corrector. It is found that the resulting MUSTA schemes reproduce the Godunov upwind scheme for the model hyperbolic equation for any number of stages. For non-linear systems the MUSTA scheme with one or two stages gives results that are indistinguishable from those of *complete* Riemann solvers, such as the exact Riemann solver, Roe's approximate Riemann solver [18] and Toro's approximate Riemann solver HLLC [29]. For the model hyperbolic equation the resulting *simultaneous updating* schemes are linearly stable in two and three space dimensions and the stability region is identical to that of the Godunov upwind method. We recall this is not the case for established centred schemes, such as the Lax-Friedrichs (not the so-called local Lax-Friedrichs, or more precisely, the Rusanov scheme) and the FORCE scheme [28]. We extend the new MUSTA schemes to multi-dimensional non-linear hyperbolic systems and to higher order of accuracy in the frame of TVD and WENO schemes. We assess the schemes on carefully chosen test problems for the one, two and three-dimensional Euler equations for compressible materials, including the computation of shock waves in compressible liquids.

The rest of the paper is organized as follows: Sect. 2 introduces the finite volume frame work and recalls well-known numerical fluxes. In Sect. 3 we present a new numerical flux. In Sect. 4 we incorporate this flux into the MUSTA framework. In Sect. 5 we illustrate the application of the proposed schemes to the solution of the Euler equations with general equations of state and present one-dimensional numerical examples for ideal and covolume gases. In Sect. 6 we extend the schemes to multi-dimensional problems in the frame of the high-order WENO methods and apply the schemes to a double Mach reflection problem in two dimensions and to an underwater explosion problem in three space dimensions. Conclusions are drawn in Sect. 7.

2 The Framework

Finite volume and discontinuous Galerkin finite element methods rely on a monotone, first-order intercell numerical flux, the building block of the schemes. Here we are concerned with numerical fluxes in the frame of the finite volume approach.

2.1 Finite Volume Schemes

For the purpose of this section it is sufficient to consider a time-dependent non-linear system of hyperbolic conservation laws in two space dimensions

$$\partial_t \mathbf{Q} + \partial_x \mathbf{F}(\mathbf{Q}) + \partial_y \mathbf{G}(\mathbf{Q}) = \mathbf{0} \,, \tag{1}$$

in which $\mathbf{Q}$ is the vector of conserved variables and $\mathbf{F} = \mathbf{F}(\mathbf{Q})$ and $\mathbf{G} = \mathbf{G}(\mathbf{Q})$ are the vectors of fluxes in the Cartesian coordinate directions x and y respectively. In the presence of discontinuous solutions one uses the integral form of (1), which is obtained, for example, by integrating (1) on a control volume V with boundary A, leading to

$$\frac{d}{dt}\int\int_V \mathbf{Q}\, dV = -\int_A (\mathbf{F}, \mathbf{G}) \cdot \mathbf{n} dA \,. \tag{2}$$

Here $\mathbf{n}$ is the unit vector normal to the boundary A pointing in the outward direction. In the finite volume approach one does not require a change of coordinates, such as body-fitted coordinates, to deal with domains whose boundaries are not aligned with the Cartesian directions. Discretization can be performed directly in physical space. Assuming the domain of interest has been discretized by an appropriate mesh, we then apply (2) to a finite volume, or cell, V_i to construct numerical schemes. In particular, a fully discrete finite volume scheme reads:

$$\mathbf{Q}_i^{n+1} = \mathbf{Q}_i^n - \frac{\Delta t}{\Delta V_i} \sum_{s=1}^{N} L_s \mathbf{T}_s^{-1} \mathbf{F}_{(i,s)} \,. \tag{3}$$

Here $\mathbf{Q}_i^n$ is the integral average of $\mathbf{Q}$ in volume V_i at time level n, ΔV_i is the area of V_i, Δt is the time step, N is the total number of faces of V_i, L_s is the length of face s, $\mathbf{T}_s$ is the rotation matrix corresponding to side s and $\mathbf{T}_s^{-1}$ is its inverse, $\mathbf{F}_{(i,s)}$ is the numerical flux for face s in the direction d normal to it, and is obtained by solving the Riemann problem in the direction d, namely

$$\left.\begin{array}{l} \partial_\tau \mathbf{Q} + \partial_d \mathbf{F}(\mathbf{Q}) = \mathbf{0} \,, \\ \\ \mathbf{Q}(d,0) = \left\{ \begin{array}{lll} \mathbf{Q}_i^0 & \equiv \mathbf{T}_s(\mathbf{Q}_i^n) & \text{if} \quad d < 0 \,, \\ \mathbf{Q}_s^0 & \equiv \mathbf{T}_s(\mathbf{Q}_s^n) & \text{if} \quad d > 0 \,. \end{array} \right. \end{array}\right\} \tag{4}$$

Here $\tau = t - t^n$ is local time; $\mathbf{Q}_s^n$ is the integral average of the conserved variable vector in the control volume adjacent to V_i having s as a common face. T_s aligns the original initial data in the normal direction d to the interface s, prior to solving the Riemann problem. The inverse matrix T_s^{-1} restores back the flux information to the Cartesian frame.

From this point on, the discussion on the numerical flux in an arbitrary direction d can be reduced to that of the *augmented* one-dimensional problem in the x-direction, say, without losing generality.

2.2 Numerical Fluxes

Consider the $m \times m$ one-dimensional system of hyperbolic conservation laws

$$\partial_t \mathbf{Q} + \partial_x \mathbf{F}(\mathbf{Q}) = \mathbf{0} \,, \tag{5}$$

where $\mathbf{Q}$ is a vector of m components, the conserved variables, and $\mathbf{F}(\mathbf{Q})$ is the corresponding vector of fluxes. The finite volume scheme to solve (5) reads

$$\mathbf{Q}_i^{n+1} = \mathbf{Q}_i^n - \frac{\Delta t}{\Delta x}[\mathbf{F}_{i+\frac{1}{2}} - \mathbf{F}_{i-\frac{1}{2}}] \,, \tag{6}$$

where $\mathbf{F}_{i+\frac{1}{2}}$ is the numerical flux, Δx is the length of the *control volume* and Δt is the time step.

Godunov's upwind method [7] defines the intercell numerical flux $\mathbf{F}_{i+\frac{1}{2}}$ in terms of the solution, if available, of the corresponding Riemann problem

$$\left.\begin{array}{l} \partial_t \mathbf{Q} + \partial_x \mathbf{F}(\mathbf{Q}) = \mathbf{0} \ , \\ \\ \mathbf{Q}(x,0) = \left\{ \begin{array}{ll} \mathbf{Q}_i^n & \text{if} \quad x < 0 \ , \\ \mathbf{Q}_{i+1}^n & \text{if} \quad x > 0 \ . \end{array} \right. \end{array} \right\} \tag{7}$$

The so-called *Riemann fan* in the $x-t$ plane consists of $m+1$ constant states separated by m wave families, each one associated with a real eigenvalue $\lambda^{(k)}$. The similarity solution of (7) depends on the ratio x/t and is denoted by $\mathbf{Q}_{i+\frac{1}{2}}(x/t)$. The Godunov intercell numerical flux is found by first evaluating $\mathbf{Q}_{i+\frac{1}{2}}(x/t)$ at $x/t = 0$, that is along the t-axis, and then evaluating the physical flux vector $\mathbf{F}(\mathbf{Q})$ in (7) at $\mathbf{Q}_{i+\frac{1}{2}}(0)$, namely

$$\mathbf{F}_{i+\frac{1}{2}}^{GodU} = \mathbf{F}(\mathbf{Q}_{i+\frac{1}{2}}(0)) \ . \tag{8}$$

The exact solution of (7) for complicated systems will generally involve the iterative solution of a non-linear system and thus in practice, whenever available, one uses approximate Riemann solvers. For a review on Riemann solvers see, for example, [27].

Non-upwind (or centred, or symmetric) schemes do not explicitly utilize wave propagation information and are thus simpler and more generally applicable. Commonly, the numerical fluxes can be computed explicitly as algebraic functions of the initial condition in (7), namely

$$\mathbf{F}_{i+\frac{1}{2}} = \mathbf{F}_{i+\frac{1}{2}}(\mathbf{Q}_i^n, \mathbf{Q}_{i+1}^n) \ . \tag{9}$$

One may interpret centred fluxes as resulting from a *low-level approximation* to the solution of the Riemann problem (7), in which the Riemann fan *is not opened*. Two classical centred fluxes are the Lax-Friedrichs flux

$$\mathbf{F}_{i+\frac{1}{2}}^{LF} = \frac{1}{2}[\mathbf{F}(\mathbf{Q}_i^n) + \mathbf{F}(\mathbf{Q}_{i+1}^n)] - \frac{1}{2}\frac{\Delta x}{\Delta t}[\mathbf{Q}_{i+1}^n - \mathbf{Q}_i^n] \tag{10}$$

and the two-step Lax-Wendroff flux

$$\mathbf{F}_{i+\frac{1}{2}}^{LW} = \mathbf{F}(\mathbf{Q}_{i+\frac{1}{2}}^{LW}) \ , \quad \mathbf{Q}_{i+\frac{1}{2}}^{LW} = \frac{1}{2}[\mathbf{Q}_i^n + \mathbf{Q}_{i+1}^n] - \frac{1}{2}\frac{\Delta t}{\Delta x}[\mathbf{F}(\mathbf{Q}_{i+1}^n) - \mathbf{F}(\mathbf{Q}_i^n)] \ . \tag{11}$$

Another, more recent, centred flux is the FORCE flux, which was derived [26] from a deterministic interpretation of the staggered-grid version of Glimm's method [5] and results in a non-staggered one-step conservative scheme of the form (6) with intercell numerical flux

$$\mathbf{F}_{i+\frac{1}{2}}^{\text{force}} = \frac{1}{4}\left[\mathbf{F}(\mathbf{Q}_i^n) + 2\mathbf{F}(\mathbf{Q}_{i+\frac{1}{2}}^{LW}) + \mathbf{F}(\mathbf{Q}_{i+1}^n) - \frac{\Delta x}{\Delta t}\left(\mathbf{Q}_{i+1}^n - \mathbf{Q}_i^n\right)\right] \ , \tag{12}$$

with $\mathbf{Q}_{i+\frac{1}{2}}^{LW}$ as in (11). For further details on the FORCE flux see [27] and [28]. See also [1], where convergence is proved for the case of two non-linear hyperbolic systems, namely the equations of isentropic gas dynamics and the shallow water equations with a bottom slope source term.

3 Generalized FORCE Fluxes

Here we construct generalizations of the FORCE flux (12) by considering convex averages of fluxes (10) and (11). To this purpose we first consider the model linear advection equation

$$\partial_t q + \lambda \partial_x q = 0 \ , \ \ \lambda \text{: constant} \ . \tag{13}$$

The physical flux function is a linear function of the unknown q, namely $f(q) = \lambda q$. The corresponding conservative scheme is written as

$$q_i^{n+1} = q_i^n - \frac{\Delta t}{\Delta x}[f_{i+\frac{1}{2}} - f_{i-\frac{1}{2}}] \ , \tag{14}$$

for which the Lax-Wendroff, Lax-Friedrichs and FORCE fluxes are

$$f^{lw}_{i+\frac{1}{2}} = \frac{1}{2}(1+c)(\lambda q_i^n) + \frac{1}{2}(1-c)(\lambda q_{i+1}^n) \ , \tag{15}$$

$$f^{lf}_{i+\frac{1}{2}} = \frac{(1+c)}{2c}(\lambda q_i^n) - \frac{(1-c)}{2c}(\lambda q_{i+1}^n) \ , \tag{16}$$

and

$$f^{force}_{i+\frac{1}{2}} = \frac{(1+c)^2}{4c}(\lambda q_i^n) - \frac{(1-c)^2}{4c}(\lambda q_{i+1}^n) \ , \tag{17}$$

where c is the CFL or Courant number

$$c = \frac{\lambda \Delta t}{\Delta x} \ . \tag{18}$$

Now consider a generalization of the FORCE flux, called GFORCE, given by the convex average

$$f^{gf}_{i+\frac{1}{2}} = \omega f^{lw}_{i+\frac{1}{2}} + (1-\omega) f^{lf}_{i+\frac{1}{2}} \ , \tag{19}$$

with the weight ω satisfying $0 \le \omega \le 1$. Written in full, the generalized FORCE flux for (13) reads

$$f^{gf}_{i+\frac{1}{2}} = \frac{1}{2}(1+c)\left[\frac{(1-c)\omega + 1}{c}\right](\lambda q_i^n) + \frac{1}{2}(1-c)\left[\frac{(1-c)\omega - 1}{c}\right](\lambda q_{i+1}^n) \ . \tag{20}$$

In the $c-\omega$ plane of Fig. 1 we show special curves $\omega(c)$ that when substituted into (20) reproduce well-known numerical fluxes. For example, the bottom horizontal line with constant weight $\omega = 0$ gives the Lax-Friedrichs flux. The top horizontal line with constant weight $\omega = 1$ gives the Lax-Wendroff flux. For the constant weight $\omega = \frac{1}{2}$ we reproduce the FORCE flux (12) for non-linear systems (5) and the flux (17) for the linear advection equation (13).

By comparing the coefficients of the flux (20) with those of the Godunov upwind flux

$$f^{GodU}_{i+\frac{1}{2}} = \begin{cases} \lambda q_i^n & \text{if} \quad \lambda > 0 \ , \\ \lambda q_{i+1}^n & \text{if} \quad \lambda < 0 \ , \end{cases} \tag{21}$$

we obtain the Courant number dependent weight given by

$$\omega_g(c) = \frac{1}{1+|c|} \ , \tag{22}$$

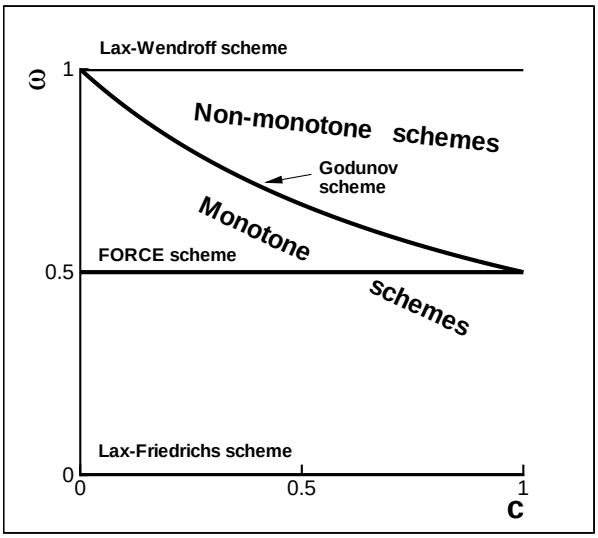

Figure 1: Numerical fluxes as convex averages of the Lax-Friedrichs (LF) and Lax-Wendroff (LW) fluxes in the $c - \omega$ plane. Here c is Courant number and ω is weight, whose constant values 0, $\frac{1}{2}$ and 1 reproduce the Lax-Friedrichs, FORCE and Lax-Wendroff fluxes; $\omega = \frac{1}{1+|c|}$ reproduces the Godunov upwind method

.

for which the generalized FORCE flux (20) reproduces identically the Godunov's upwind flux. For any constant value of the weight ω, with $0 \leq \omega \leq 1$ we have a 3-point scheme (14) whose coefficient of numerical dissipation is

$$\alpha_{gf} = \frac{1}{2}\left[\frac{(1-c^2)(1-\omega)}{c}\right]\lambda\Delta x \ , \tag{23}$$

which varies linearly with ω, it is a maximum for the Lax-Friedrichs flux ($\omega = 0$) and zero for the Lax-Wendroff flux ($\omega = 1$).

The curve $\omega_g(c)$ divides the unit square of Fig. 1 into two subregions. The region associated with weights lying above the Godunov weight $\omega_g(c)$ contains non-monotone schemes and the region below $\omega_g(c)$ contains monotone schemes. The range of *constant* weights ω (no dependence on c), with $0 \leq \omega \leq \frac{1}{2}$, defines a sub-class of monotone schemes, with the FORCE flux (17) corresponding to the limiting case $\omega = \frac{1}{2}$, which is the scheme with the smallest numerical dissipation within the class, and thus the optimal scheme, for which no dependence on c (no upwind information) is required.

For any constant weight ω, with $\frac{1}{2} < \omega \leq 1$, we enter the non-monotone region, for the larger range of Courant numbers. Thus the only way to improve upon the FORCE flux, that is to reduce its numerical viscosity further, is to take a weight that goes above $\frac{1}{2}$. But in order to preserve also monotonicity such weight would have to depend on the Courant number c. This in turn would mean that the scheme would have to depend on *wave propagation information*, that is on *upwinding*. As it happens, the curve $\omega(c)$ that would give a monotone scheme with the smallest truncation error would be $\omega_g(c)$ given by (22), which corresponds precisely to the Godunov's upwind flux (21), with coefficient of numerical viscosity given by

$$\alpha_{god} = \frac{1}{2}(1-|c|)\lambda\Delta x \ . \tag{24}$$

In Fig. 1 there is region that may be described as a *triangle* with a curved hypotenuse that lies above $\omega = \frac{1}{2}$ and below $\omega = \omega_g(c) = \frac{1}{1+|c|}$. This region represents additional numerical dissipation to that of the optimal centred scheme FORCE with constant $\omega = \frac{1}{2}$. This extra dissipation exists because of *non-upwinding* and in order to dispose of it, we require schemes with some dependence on the Courant number (upwinding).

In this paper we present two ways of disposing of the additional numerical dissipation of the optimal centred method, FORCE. The simplest way is through the use of the GFORCE approach (19), which for non-linear hyperbolic systems (5) as solved by (6) has numerical flux

$$\mathbf{F}^{GF}_{i+\frac{1}{2}} = \Omega_{loc}\mathbf{F}^{LW}_{i+\frac{1}{2}} + (1-\Omega_{loc})\mathbf{F}^{LF}_{i+\frac{1}{2}} \, , \tag{25}$$

where Ω_{loc} has the form

$$\Omega_{loc} = \frac{1}{1+C_{loc}} \, . \tag{26}$$

C_{loc} is a prescribed local Courant number coefficient, with $0 < C_{loc} \leq 1$, from which a local time step is computed. See section 4, algorithm (36). It is obvious that for the model equation (13) the proposed flux (25) reproduces the Godunov's upwind flux (22). The second way of recovering the region above $\omega = \frac{1}{2}$ and below $\omega = \omega_g(c) = \frac{1}{1+|c|}$ in Fig. 1 is through the use of the MUSTA approach [23] utilizing symmetric fluxes in a multi-stage predictor-corrector procedure.

4 MUSTA Fluxes

In computing an intercell numerical flux for the conservative scheme (6) one knows the governing differential equations in (7) and the initial condition $\mathbf{Q}^n_i$, $\mathbf{Q}^n_{i+1}$ either side of the interface $i+\frac{1}{2}$. In other words, the point of departure in computing the numerical flux in precisely the Riemann problem (7). Recall also that the optimal monotone numerical flux is that obtained from the solution of the Riemann problem (7) followed by the flux evaluation (8), that is the Godunov's upwind flux. Alternatively, one could use the MUSTA approach [23], whereby known flux functions, such as the newly proposed flux (25), could be used in a predictor-corrector fashion, avoiding in this manner the explicit solution of the Riemann problem (7).

4.1 The MUSTA Predictor-Corrector Approach

The MUSTA approach may be interpreted as a method in which the Riemann problem (7) is solved numerically on a coarse mesh on the $d-\tau$ plane, see Fig. 2. We define a *local domain* of length D and a *local mesh* of $2m$ cells, with m a positive integer. The local mesh has size $\Delta d = \frac{1}{2}D/m$ and the initial condition becomes

$$\mathbf{Q}^{(0)}_l = \begin{cases} \mathbf{Q}^n_i & \text{if} \quad l \leq 0 \, , \\ \\ \mathbf{Q}^n_{i+1} & \text{if} \quad l > 0 \, , \end{cases} \tag{27}$$

for $l = -m+1, \ldots, m$. The interface $x_{i+\frac{1}{2}}$ in the *global mesh* for scheme (6) corresponds to the interface $\frac{1}{2}$ in the local mesh.

For the *local time marching*, or multi-staging, we use an explicit method, such as (25). This requires the prescription of a CFL coefficient, denoted by C_{loc} in (26), and the computation of a *local time step* imposing a local CFL stability condition. Concerning *local boundary conditions*,

we recall that the initial condition extends to $-\infty$ and $+\infty$ and thus we would like to have unimpeded passage of waves through the *local numerical boundaries* at $-m+1/2$ and $m+\frac{1}{2}$. We apply simple transmissive boundary conditions $\mathbf{Q}^{(k)}_{-m} = \mathbf{Q}^{(k)}_{-m+1}$ and $\mathbf{Q}^{(k)}_{m+1} = \mathbf{Q}^{(k)}_{m}$ so that the boundary fluxes are

$$\mathbf{F}^{(k)}_{-m+1/2} = \mathbf{F}(\mathbf{Q}^{(k)}_{-m+1}) \ , \quad \mathbf{F}^{(k)}_{m+\frac{1}{2}} = \mathbf{F}(\mathbf{Q}^{(k)}_{m}) \ . \tag{28}$$

4.2 The MUSTA-1 Scheme

Here we describe a practical MUSTA scheme, MUSTA-1, that uses the GFORCE flux (25) as predictor and corrector, on the simplest local mesh of 2 cells ($m = 1$) and one stage ($K = 1$) This is illustrated in Fig. 2, where the two computational cells, numbered, from left to right, as 0 (associated with $\mathbf{Q}^n_i$) and 1 (associated with $\mathbf{Q}^n_{i+1}$). The corresponding local mesh interfaces are denoted by $-1/2$, $1/2$ and $3/2$. The relevant interface $i+\frac{1}{2}$ of the conservative scheme (6) is associated with the local interface $1/2$. The boundary fluxes in Fig. 2 are shown as thin arrows, while the fluxes at the relevant interface $\frac{1}{2}$ are shown by the thicker arrows.

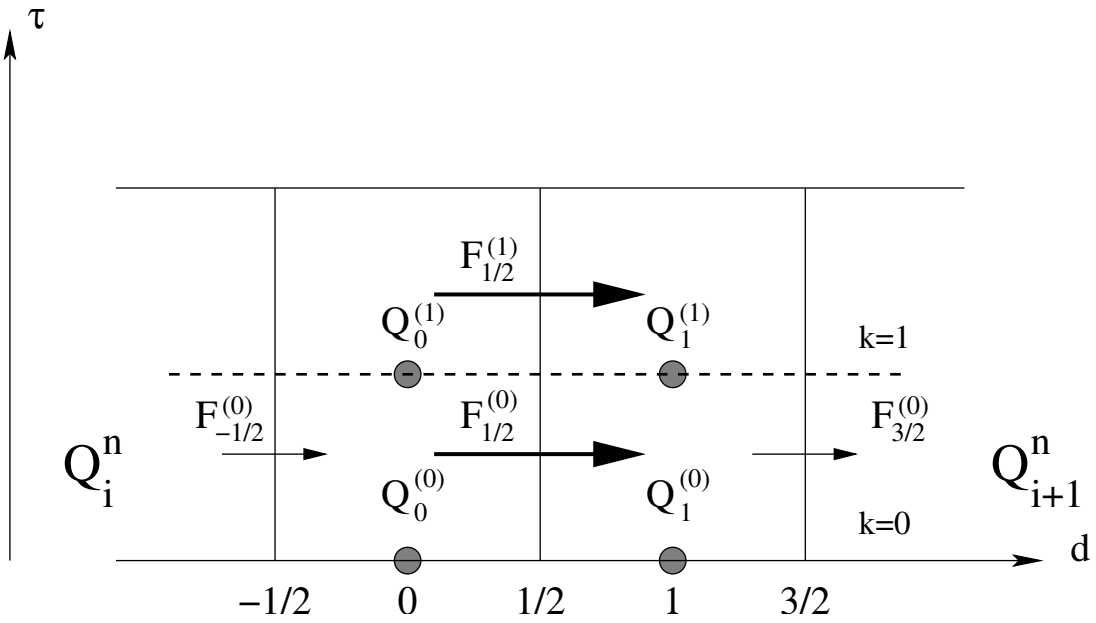

Figure 2: Illustration of the MUSTA-1 flux in the local $d-\tau$ frame.

The method is started by first prescribing a local CFL coefficient C_{loc}. As we use the GFORCE flux as predictor, the CFL coefficient satisfies $0 < C_{loc} \leq 1$. Then we compute the weight Ω_{loc}, for a prescribed C_{loc}, according to (26). The initial conditions are set as follows

$$\mathbf{Q}^{(0)}_0 = \mathbf{Q}^n_i \ , \quad \mathbf{Q}^{(0)}_1 = \mathbf{Q}^n_{i+1} \ . \tag{29}$$

Then, one estimates a local maximum wave speed $S^{(0)}$, based on the local initial condition, that is the states $\mathbf{Q}^{(0)}_0$ and $\mathbf{Q}^{(0)}_1$. This part of the method depends crucially on the particular hyperbolic system of interest. Then, a *local time step* is computed

$$\Delta\tau^{(0)} = C_{loc}\frac{\Delta d}{S^{(0)}} \ . \tag{30}$$

The transmissive boundary conditions applied result in the boundary fluxes

$$\mathbf{F}^{(0)}_{-1/2} = \mathbf{F}(\mathbf{Q}^{(0)}_0) \ , \quad \mathbf{F}^{(0)}_{3/2} = \mathbf{F}(\mathbf{Q}^{(0)}_1) \ . \tag{31}$$

The intercell numerical flux (25) corresponding to the interface of interest is

$$\mathbf{F}^{(0)}_{1/2} = \Omega_{loc}\mathbf{F}^{LW}_{1/2}(\mathbf{Q}^{(0)}_0, \mathbf{Q}^{(0)}_1, \Delta\tau^{(0)}, \Delta d) + (1-\Omega_{loc})\mathbf{F}^{LF}_{1/2}(\mathbf{Q}^{(0)}_0, \mathbf{Q}^{(0)}_1, \Delta\tau^{(0)}, \Delta d) \ . \tag{32}$$

Then we advance in local time according to

$$\mathbf{Q}^{(1)}_0 = \mathbf{Q}^{(0)}_0 - \frac{\Delta\tau^{(0)}}{\Delta d}[\mathbf{F}^{(0)}_{1/2} - \mathbf{F}^{(0)}_{-1/2}] \ , \quad \mathbf{Q}^{(1)}_1 = \mathbf{Q}^{(0)}_1 - \frac{\Delta\tau^{(0)}}{\Delta d}[\mathbf{F}^{(0)}_{3/2} - \mathbf{F}^{(0)}_{1/2}] \ . \tag{33}$$

Having computed the predicted values $\mathbf{Q}^{(1)}_0$ and $\mathbf{Q}^{(1)}_1$ we compute a corrected flux. First we compute a new local wave speed $S^{(1)}$ and an associated time step $\Delta\tau^{(1)}$ as in (30). Then the corrected flux function $\mathbf{F}^{(1)}_{3/2}$ is computed as in (32), namely

$$\mathbf{F}^{(1)}_{1/2} = \Omega_{loc}\mathbf{F}^{LW}_{1/2}(\mathbf{Q}^{(1)}_0, \mathbf{Q}^{(1)}_1, \Delta\tau^{(1)}, \Delta d) + (1-\Omega_{loc})\mathbf{F}^{LF}_{1/2}(\mathbf{Q}^{(1)}_0, \mathbf{Q}^{(1)}_1, \Delta\tau^{(1)}, \Delta d) \ . \tag{34}$$

Finally we set the numerical flux $\mathbf{F}_{i+1/2} = \mathbf{F}^{(1)}_{1/2}$ and use it in the conservative formula (6).

As argued earlier, the MUSTA fluxes are meant to use a very coarse approximation to the numerical solution of the Riemann problem (7). The case of Fig. 2 (MUSTA-1) uses a *mesh* of only two cells and very simple *transmissive* boundary conditions, which provide the left and right fluxes $\mathbf{F}(\mathbf{Q}^{(k)}_0)$ and $\mathbf{F}(\mathbf{Q}^{(k)}_1)$. In general, for a larger number of stages we must consider a larger *local* domain and a larger *local* mesh so that the numerical boundaries are sufficiently far away from the relevant interface. Note that at stage $k = 1$ we already have $\mathbf{Q}^{(1)}_0 \neq \mathbf{Q}^{(0)}_0$ (the left state at $-\infty$) and $\mathbf{Q}^{(1)}_1 \neq \mathbf{Q}^{(0)}_1$ (the right state at $+\infty$). Therefore, the boundary fluxes may not prevent the influence of the numerical boundaries, where waves will then be produced and which will then propagate back to the interface, affecting the multi-staging procedure for $\mathbf{Q}^{(k)}_0$ and $\mathbf{Q}^{(k)}_1$. Therefore, if a large number of stages is desired, one must consequently increase appropriately the domain and the mesh. If a convergent numerical *predictor* is used, then one would expect that as the number of mesh points p and the number of stages k tend to ∞ we should expect that the states $\mathbf{Q}^{(k)}_0$ and $\mathbf{Q}^{(k)}_1$ would be close to the exact solution of the Riemann problem (7) at the interface and that the *corrected* numerical flux $\mathbf{F}^{(K)}_{1/2}(\mathbf{Q}^{(K)}_0, \mathbf{Q}^{(K)}_1, \Delta\tau^{(K)}, \Delta d)$ would be close to that of the Godunov upwind flux (8) using the exact solution of the Riemann problem.

4.3 Properties of the MUSTA Schemes

As already remarked, for the linear advection equation (13) the generalized FORCE scheme (19) reproduces identically the Godunov upwind flux (21) when $\omega = \frac{1}{1+|c|}$. Here we note that this property also holds for the MUSTA schemes based on the GFORCE flux (20) used as predictor and corrector. This property is easily proved for an arbitrary number of stages K. Table 1 illustrates the evolution of the initial data states q_L, q_R in the MUSTA multi-staging procedure. For a positive wave speed λ the left state q_L remains unaltered, while the right state q_R changes at every stage. However, the relevant intercell flux $f^{(k)}_{1/2}$ remains constant and equal to that of the Godunov's upwind scheme.

k	$q_0^{(k)}$	$q_1^{(k)}$	$f_{-1/2}^{(k)}$	$f_{1/2}^{(k)}$	$f_{3/2}^{(k)}$
0	q_L	q_R	λq_L	λq_L	λq_R
1	q_L	$cq_L + (1-c)q_1^{(0)}$	λq_L	λq_L	$\lambda q_1^{(1)}$
2	q_L	$cq_L + (1-c)q_1^{(1)}$	λq_L	λq_L	$\lambda q_1^{(2)}$
3	q_L	$cq_L + (1-c)q_1^{(2)}$	λq_L	λq_L	$\lambda q_1^{(3)}$

Table 1: The MUSTA flux for linear advection using the GFORCE scheme as predictor and corrector, for 3 stages. At each stage, the Godunov upwind flux is reproduced identically, see column 5.

The MUSTA-1 scheme has the following properties, when applied to the one-dimensional model hyperbolic equation (13),

- The scheme has *linear stability* condition

$$0 < |c| \leq 1 \quad \text{in one dimension} . \tag{35}$$

- The scheme is *monotone* under the above stability condition and has the smallest truncation error within the class of monotone schemes. The leading term of the truncation error has coefficient as given by (24).

- When extended to multidimensional problems in a straightforward unsplit form (see Sect. 6) the scheme has the following *linear stability* conditions:

$$c_x + c_y \leq 1 \quad \text{in two dimensions} , \quad c_x + c_y + c_z \leq 1 \quad \text{in three dimensions} , \tag{36}$$

  where c_x, c_y and c_z are directional CFL numbers. See Sect. 5 for more details.

5 MUSTA Fluxes for Compressible Materials

An attractive feature of the MUSTA numerical flux is the easy with which one can solve complicated problems. As seen in (34) the computation of the numerical flux only involves evaluation of the normal flux $\mathbf{F}$, without having to solve directly the Riemann problem (7). This means that the method can be applied to general hyperbolic systems in conservation form. The restriction imposed by a particular hyperbolic system enters in the estimation of a local maximum signal speed. We assume that sufficient information on the eigenvalues of the system is available to compute a stable time step Δt for the *global* scheme; for very complicated systems such information will probably be available by numerical means. Therefore, such procedure can also be applied locally to estimate the speeds $S^{(k)}$ in the computation of the numerical flux. Here we illustrate the applicability of the methods via the Euler equations of gas dynamics for compressible materials with general equation of state.

5.1 The Euler Equations

The non-linear time-dependent one dimensional Euler equations are

$$\left.\begin{aligned} &\partial_t \mathbf{Q} + \partial_x \mathbf{F}(\mathbf{Q}) = \mathbf{0} \,, \\ &\mathbf{Q} = \begin{bmatrix} \rho \\ \rho u \\ E \end{bmatrix} \;; \quad \mathbf{F}(\mathbf{Q}) = \begin{bmatrix} \rho u \\ \rho u^2 + p \\ u(E+p) \end{bmatrix} \,. \end{aligned}\right\} \tag{37}$$

Here ρ, u, p and E are density, particle speed, pressure and total energy, given by

$$E = \rho(\frac{1}{2}u^2 + e) \,, \tag{38}$$

where e is the specific internal energy. The eigenvalues of (37) are easily found to be

$$\lambda_1 = u - a \,, \quad \lambda_2 = u \,, \quad \lambda_3 = u + a \,, \tag{39}$$

where a is the speed of sound in the material, which depends on the appropriate equation of state for the material.

The Euler equations (37), that govern the dynamics of wave propagation in a material, are supplemented by a thermodynamics statement as to the nature of that material, via a caloric equation of state (EOS), which is a functional (non-differential) relationship between three variables. A popular choice is the trio ρ, p and e. Another choice is furnished by the specific volume $v = 1/\rho$, pressure p and specific entropy s. The particular form of the equation of state determines the form of the sound speed a. Three forms of the equation of state and the corresponding expressions for the speed of sound are:

$$\left.\begin{aligned} p = p(\rho, e) \,, \quad a &= \sqrt{\tfrac{p}{\rho^2} p_e + p_\rho} \,, \\ e = e(\rho, p) \,, \quad a &= \sqrt{\tfrac{p}{\rho^2 e_p} - \tfrac{e_\rho}{e_p}} \,, \\ p = p(v, s) \,, \quad a &= \sqrt{-v^2 p_v} \,, \end{aligned}\right\} \tag{40}$$

where subscripts denote partial derivatives.

For hyperbolicity of the Euler equations (37) one requires the sound speed to be real, which from (40) results in the condition

$$p_v = -e_{vv}(v, s) < 0 \,. \tag{41}$$

A further restriction on the EOS results from imposing that the acoustic characteristic fields associated with the eigenvalues $\lambda_1 = u - a$ and $\lambda_3 = u + a$ be *genuinely non-linear*. This is usually known as the *convexity* condition for the Euler equations and may be expressed as

$$e_{vvv}(v, s) \neq 0 \,. \tag{42}$$

More general materials not obeying the convexity assumption may also be considered, in which case, complex wave patterns may occur, such as rarefaction shock waves and composite waves. See [15].

5.2 Examples of Compressible Materials

Upwind Godunov-type methods require the solution of the Riemann problem for (37) along with a general equation of state (40). This can be costly, complex or impossible. For background see the works of Colella and Glaz [2], Glaister [4], Menikoff and Plohr [15] and Quartapelle et al. [17], amongst others. The methods of this paper do not require such solution.

5.2.1 Covolume Gases

A generalization of the ideal gas equation of state is the so-called *covolume equation of state*

$$e = \frac{p(1-b\rho)}{\rho(\gamma-1)}\,, \quad a = \sqrt{\frac{\gamma p}{(1-b\rho)\rho}}\,, \tag{43}$$

where γ is the ratio of specific heats (assumed constant) and b is called the *covolume*, which in SI units has dimensions of $\mathrm{m^3kg^{-1}}$. The conventional ideal gas case is obtained from (43) with $b = 0$. Equation of state (43) applies to dense gases at high pressure, for which the volume occupied by the molecules themselves is no longer negligible. There is therefore a reduction in the volume available to molecular motion. Sometimes, this equation is also called the Noble-Abel equation of state. In the study of propulsion systems, gaseous combustion products at very high densities are reasonably well described by the covolume equation of state. In its simplest version the covolume b is a constant and is determined experimentally or from equilibrium thermochemical calculations. For an exact Riemann solver see [24].

5.2.2 Van der Waal Gases

The covolume EOS (43) can be further corrected to account for the forces of attraction between molecules, the van der Waal forces. These are neglected in both the ideal and covolume equations of state. Accounting for such forces results in a reduction of the pressure by an amount c/v^2, where c is a quantity that depends on the particular gas under consideration. The pressure is corrected as

$$p = \frac{RT}{v-b} - \frac{c}{v^2}\,. \tag{44}$$

Then we can write

$$(p + \frac{c}{v^2})(v-b) = RT\,, \tag{45}$$

where T is temperature. This is generally known as the *van der Waal's equation of state* for real gases. For an exact Riemann solver see Quartapelle et al. [17].

5.2.3 Compressible Liquids

Liquids at high pressures must be treated as compressible fluids [21]. Application areas of interest include nuclear-reactor technology and underwater explosions, amongst many others. The simplest choice of equation of state for compressible liquids is the modified Tait's equation of state

$$p = p(\rho) = B[(\frac{\rho}{\rho_0})^{\gamma_l} - 1]\,, \tag{46}$$

where B is a weak function of entropy, and thus is usually taken as a constant; γ_l is a constant and ρ_0 is the reference density, the density of the liquid at atmospheric pressure. The corresponding expression for the sound speed is

$$a = \sqrt{\frac{\gamma_l}{\rho}(p+B)}\,. \tag{47}$$

A more complete equation of state for liquids is the Tammann equation of state

$$p = p(\rho, e) = (\gamma-1)\rho e - \gamma p_c\,, \tag{48}$$

where the constants γ and p_c are liquid dependent. For $p_c = 0$ and $1 < \gamma < 2$ one reproduces the ideal gas equation of state obtained from setting the covolume $b = 0$ in (43). The corresponding sound speed is

$$a = \sqrt{\frac{\gamma}{\rho}(p + p_c)} \ . \tag{49}$$

For Riemann solvers see [10].

5.3 One-Dimensional Numerical Examples

In order to assess the performance of the proposed MUSTA methods we select here three test problems for the time-dependent one-dimensional Euler equations, two for ideal gases and one for covolume gases for a problem with moving boundaries. In section 6 we solve the three-dimensional Euler equations with a high order WENO scheme, for the computation of shock waves in liquids arising in underwater explosions.

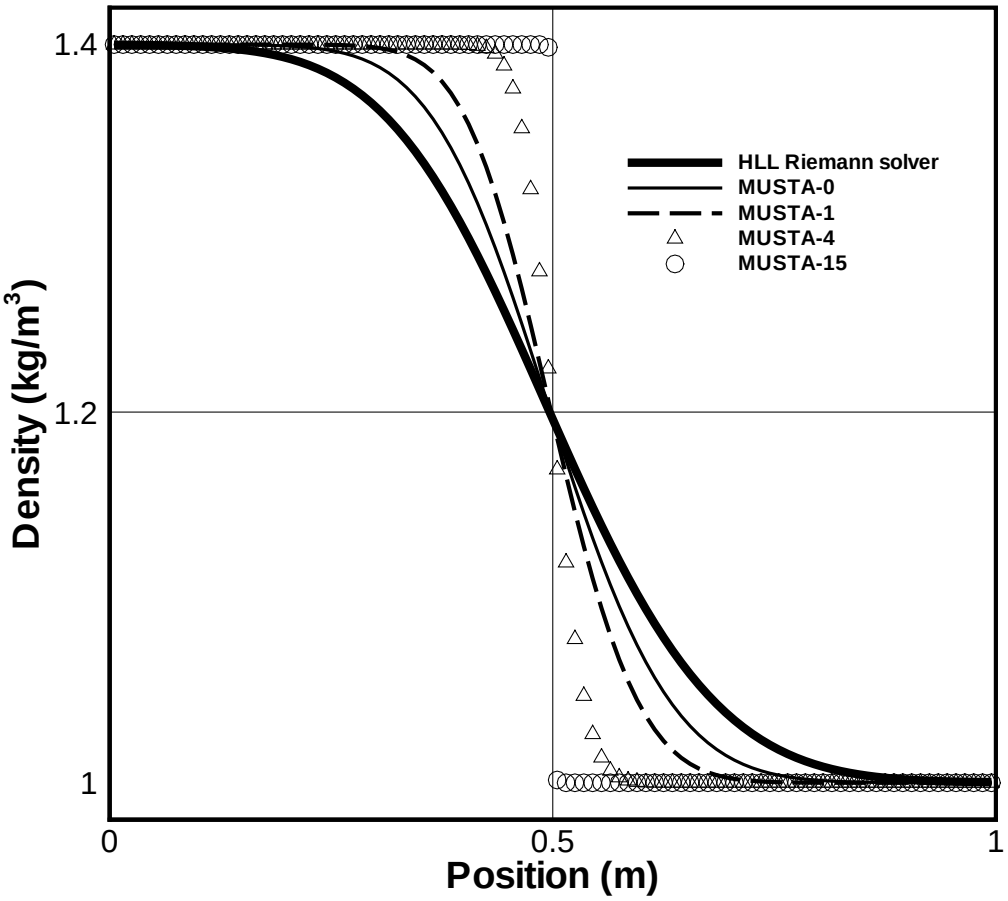

Figure 3: **Test 1: Stationary contact**. Numerical solutions for density at time $t = 2.0$ using a mesh of $M = 100$ cells and a CFL coefficient CFL=0.9. Results include those from the HLL Riemann solver, the GFORCE (MUSTA-0) flux and MUSTA-k, for $k = 1, 4, 15$.

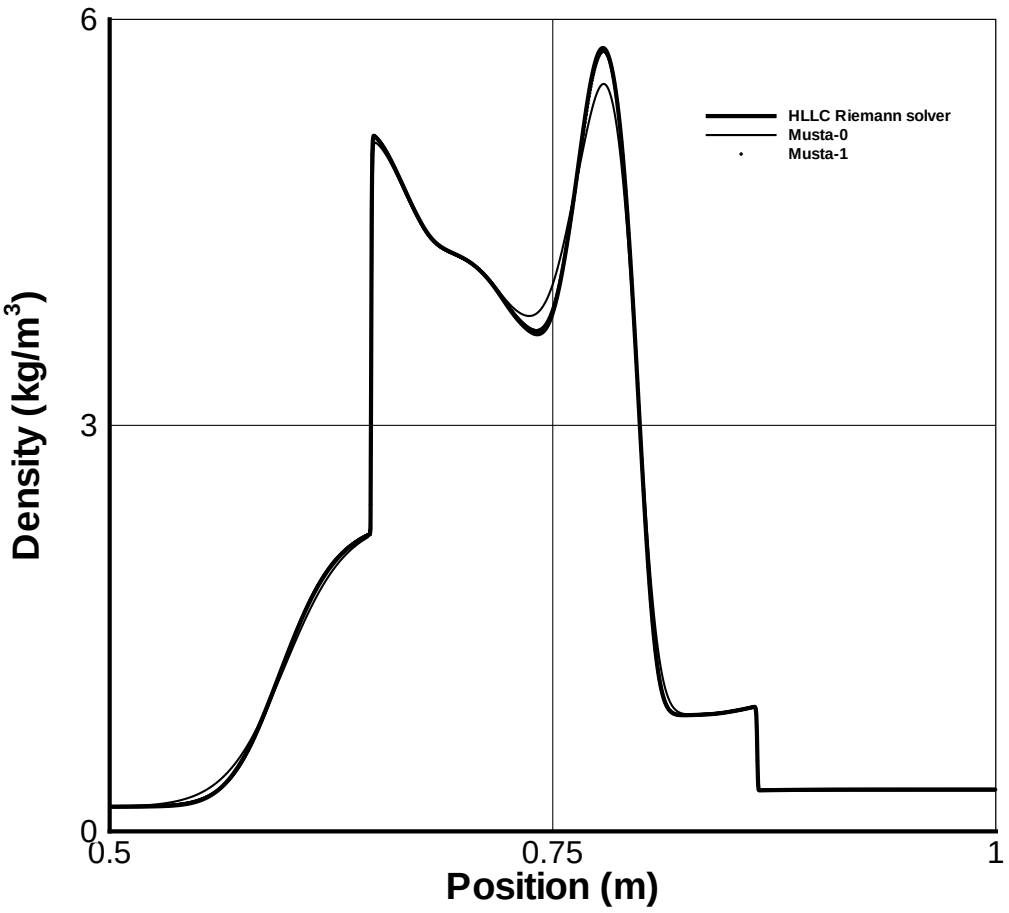

Figure 4: **Test 2: Blast wave interaction**. Numerical solutions for density at time $t = 0.038$ using a mesh of $M = 3000$ cells and a CFL coefficient CFL=0.9. Results include those from the HLLC Riemann solver (thick line), GFORCE or MUSTA-0 (thin line) and MUSTA-1 (symbol). Results from HLLC and MUSTA-1 are indistinguishable.

TEST 1: Stationary contact.

We solve the Euler equations in a domain $[0, 1]$ using the ideal gas equation of state, obtained from (43) with $\gamma = 1.4$ and $b = 0$. The initial condition consists of constant pressure $p = 1$, constant velocity $u = 1$ and a discontinuous distribution of density: $\rho = 1.4$ in $[0, 1/2]$ and $\rho = 1.0$ in $(1/2, 1]$. The purpose of this test is to assess the performance of the methods proposed in this paper for resolving *delicate features*, such as contact discontinuities, for which most numerical methods have large numerical dissipation, being the largest for the case in which the wave is stationary. Numerical results are shown in Fig. 3. The exact solution consists of an isolated stationary contact discontinuity positioned at $x = 1/2$. As the reference numerical solution we take that of the Godunov method in conjunction with the popular (incomplete) HLL Riemann solver [9], along with very accurate wave speed estimates [27]; it is seen that the contact discontinuity is smeared very badly. The next more accurate result is that from *GFORCE* (or MUSTA-0). It is surprising to see that a particular linear combination (25) of

symmetric fluxes produces more accurate results than the HLL Riemann solver. The MUSTA-k schemes give again more accurate results; realistic values of k are $k = 1$ and $k = 2$, which give acceptable results. For the limiting case of $k = 15$ (unrealistic) one obtains the exact solution, see Fig. 3. We note that a complete Riemann solver that includes all waves of the structure of the exact solution, such as Roe's [18] and HLLC [29], for example, will recognize exactly this isolated stationary contact.

TEST 2: Blast wave interaction.

We solve the Euler equations in a domain $[0, 1]$, using the ideal gas equation of state, obtained from (43) with $\gamma = 1.4$ and $b = 0$. The initial condition [31] consists of constant density $\rho = 1$, constant velocity $u = 0$ and a discontinuous distribution of pressure: $p_L = 1000$ in $[0, 1/10]$, $p_M = 0.01$ in $(1/10, 9/10]$ and $p_R = 100$ in $(9/10, 1]$. For a detailed discussion on the solution of this problem see [31]. The purpose of this test is to assess the robustness and accuracy of the proposed methods for resolving very strong shock waves and multiple wave-wave and wave-boundary interactions. Numerical results for density are shown in Fig. 4. The reference numerical solution is that obtained from the Godunov method in conjunction with the (complete) HLLC Riemann solver [29], [27] (thick line). We note here that the results with the exact Riemann solver are identicall to those with HLLC. The result from the *GFORCE* (or MUSTA-0) scheme (25) (thin line) is almost as accurate as that of the HLLC Riemann solver and the result of MUSTA-1 (symbol) is indistinguishable from that of HLLC and the symbols are thus covered by the thick line.

TEST 3: Lagrange's problem with covolume.

The Lagrange's problem is a test for both Euler solvers with the covolume equation of state (43) as well as for testing moving boundary schemes. The problem consists of a tube of constant, circular cross-sectional area with a combustion chamber at the left end, filled with stationary combustion products at high density and pressure. At the right-hand end of the combustion chamber is the base of a piston of a given mass, assumed to occupy the full cross-sectional area of the tube, so that the gases are sealed. See Table 2. A theoretical solution to this problem was obtained by Love and Pidduck [14], of which Table 3 gives the solution at 10 values of time.

Tube total length of tube	7.698 (m)
Tube radius	0.075 (m)
Combustion chamber length	1.698 (m)
Initial gas density in chamber	400.0 (kg/m^3)
Initial gas speed in chamber	0 (m/s)
Initial gas pressure in chamber	621.0 (MPa)
Ratio of specific heats	11/9
Covolume	0.001 (m^3/kg)
Total mass of piston	50 (kg)

Table 2. Data for the Lagrange's problem.

Time, ms	Piston base position	Piston speed	Breech pressure	Piston base pressure
0.4772	1.72165	99.64	621.06	554.17
0.9544	1.78965	187.70	621.06	499.84
1.4785	1.91165	275.40	507.10	451.01
2.1170	2.11965	371.80	408.84	402.27
2.8980	2.45165	466.20	325.19	291.26
3.8590	2.94065	550.40	255.95	212.84
5.1540	3.71865	632.50	169.46	150.53
7.1370	5.05365	718.30	106.50	101.10
10.2300	7.41665	801.30	63.74	57.04
10.5800	7.69765	807.70	* 60.88	54.19

Table 3. Theoretical solution for the Lagrange's problem [14]. Value * obtained from interpolation procedure using a reference numerical solution with the WAF scheme [25].

At time $t = 0$ one assumes instantaneous combustion in the chamber and the piston is free to move under the action of the high pressure. At time $t = 10.58\ ms$ the base of the piston leaves the end of the tube at $x = 7.698\ m$ at an exit speed of $V = 807.70\ m/s$. Fig. 5 show results, as functions of time, for the piston base position, the piston speed, the pressure at the centre of the tube at $x = 0$ (the breech), and the pressure at the base of the piston. The numerical solution (full line) is compared with the theoretical solution (symbols) given in Table 3. The numerical results were obtained from a TVD extension of the MUSTA scheme, starting the computations with an initial mesh of $M = 100$ cells and then adding *cut cells* as the computational domain was enlarged due to the traveling of the piston towards the exit of the tube. As seen in Fig. 5 the agreement between the numerical and the theoretical solution is satisfactory.

5.4 Extensions of MUSTA

The MUSTA fluxes can be used in the frame of existing finite volume and discontinuous Galerkin approaches to obtain schemes of higher order of accuracy, along with various ways of constructing non-oscillatory versions of the schemes.

In two and three space dimensions one can construct *unsplit, or simultaneous updating* schemes of the form (3), with MUSTA-type intercell fluxes. Any existing finite volume scheme based on some Riemann solver can be used by simply replacing the Godunov-type flux by a MUSTA flux. In the context of unsplit finite volume methods for multi-dimensional problems it is worth remarking that centred fluxes such as Lax-Friedrichs (10) (not to be mistaken with Rusanov's flux [19]) and the FORCE flux (12) lead to schemes that are linearly, unconditionally unstable [28]. Split versions may produce stable schemes, but these will not be suitable for unstructured meshes or for very-high order extensions in multiple space dimensions.

The multi-staging process of the MUSTA approach results in numerical fluxes that give unsplit schemes that have identically the same stability region as the simple unsplit Godunov first-order upwind method, as shown in section 6. In fact the GFORCE flux (MUSTA-0) also enjoys this very desirable property for multi-dimensional problems.

The MUSTA fluxes can be used to construct schemes of very high order of accuracy in space and time. In section 6 we illustrate this in the frame of WENO schemes with Runge-Kutta time stepping as applied to the three-dimensional Euler equations for compressible liquids.

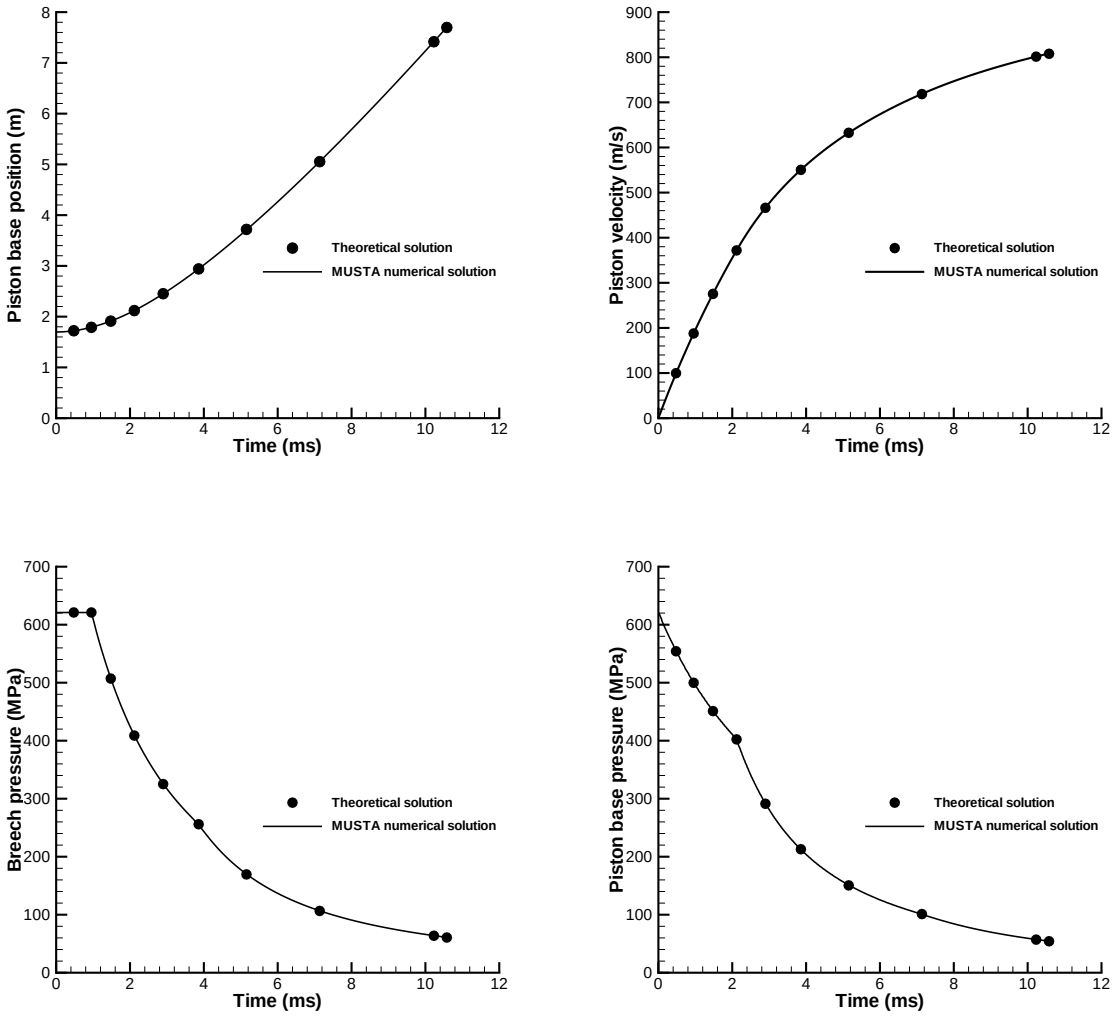

Figure 5: **Test 3: Lagrange's problem with covolume.** Numerical (line) and theoretical (symbol) solution as function of time for piston base position, piston speed, pressure at breech and pressure at the base of the piston.

6 MUSTA Fluxes in High-Order WENO Schemes

In this section we use the MUSTA fluxes constructed in previous sections as the building block in the state-of-art weighted essentially non-oscillatory (WENO) schemes. For a detailed description of finite-volume WENO schemes in two space dimensions see [20] and references therein. Here we use its three dimensional extension reported in [22]. In all examples fifth-order reconstruction and third-order time integrations are used, see [20, 22] for details. We note that in 2D the variant of the WENO scheme from [22] is different from that of [20] in that it uses a two-point Gaussian quadrature instead of a three point one.

6.1 Linear Stability of the Multi-Dimensional Schemes

We first perform a von Neumann stability analysis of the first-order MUSTA scheme as applied to the model linear advection equation with constant coefficients in three space dimensions.

$$\frac{\partial}{\partial t}q + \frac{\partial}{\partial x}f(q) + \frac{\partial}{\partial y}g(q) + \frac{\partial}{\partial z}h(q) = 0, \quad f = \lambda_1 q, \quad g = \lambda_2 q, \quad h = \lambda_3 q.$$

The scheme now reads

$$q_{ijk}^{n+1} = q_{ijk}^{n} - \frac{\Delta t}{\Delta x}\left(f_{i+1/2,jk} - f_{i-1/2,jk}\right)$$
$$-\frac{\Delta t}{\Delta y}\left(g_{ij+1/2,k} - g_{ij-1/2,k}\right) - \frac{\Delta t}{\Delta z}\left(h_{ijk+1/2} - h_{ijk-1/2}\right) ,$$

or in a more concise form:

$$q_{ijk}^{n+1} = \sum_{l,m,p=-1}^{1} b_{lmp} q_{i+l,j+m,k+p}^{n} . \tag{50}$$

We remind the reader that for the linear advection equation with constant coefficient the new

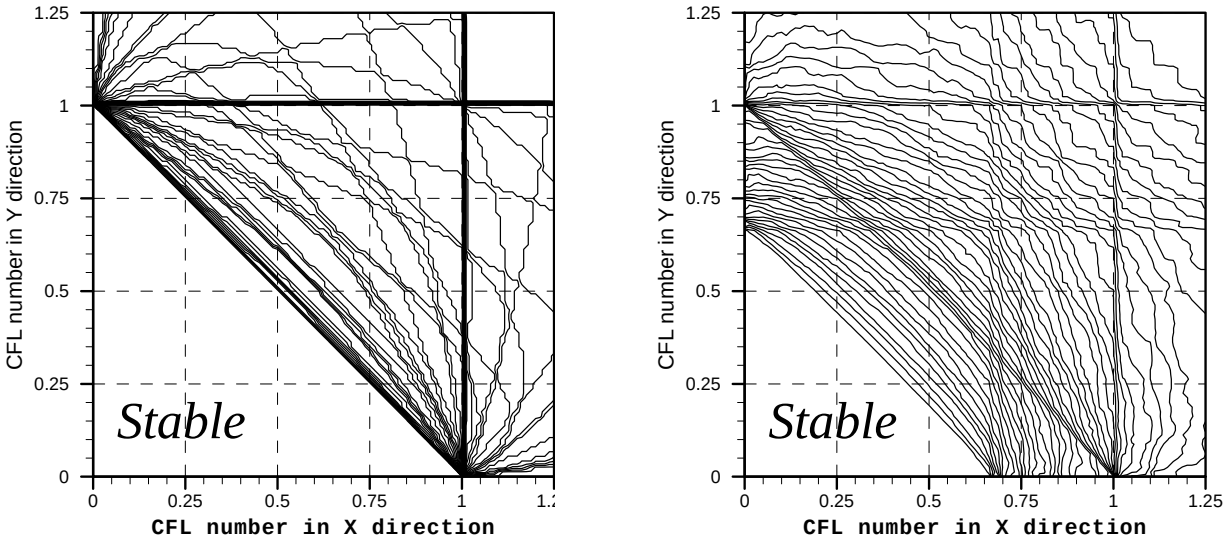

Figure 6: Stability regions for the three-dimensional Godunov scheme for $c_z = 0$ (left plot) and $c_z = 1/3$ (right plot).

MUSTA scheme of this paper reduces to the Godunov upwind method.

We then consider a *trial solution* $q_{ijk}^{n} = S^n \exp\left(I(i\alpha + j\beta + k\gamma)\right)$, where α, β and γ are phase angles in x, y and z directions respectively. Inserting the trial solution into (50) we obtain the following algebraic expression for the modulus of the amplification factor S:

$$|S|^2 = \left(\sum_{l,m,p=-1}^{1} b_{lmp}\cos\left(l\alpha + m\beta + p\gamma\right)\right)^2 + \left(\sum_{l,m,p=-1}^{1} b_{lmp}\sin\left(l\alpha + m\beta + p\gamma\right)\right)^2 .$$

For linear stability we impose the condition $|S| \leq 1$. Since the resulting expression for $|S|$ is algebraically intractable we adopt the idea of verifying the condition $|S| \leq 1$ numerically rather than analytically [28] as follows. Let us define Courant numbers for each coordinate direction

as $c_x = \lambda_1 \Delta t/\Delta x$, $c_y = \lambda_2 \Delta t/\Delta y$, $c_z = \lambda_3 \Delta t/\Delta z$. For a given set (c_x, c_y, c_z), we evaluate the amplification factor $S(c_x, c_y, c_z, \alpha, \beta, \gamma)$ for many values of the phase angles α, β, γ and record the proportion $p(c_x, c_y, c_z)$ for which $|S| \leq 1$. Then a contour plot of $p(c_x, c_y, c_z)$ in the $c_x - c_y$ plane for different values of c_z will give an indication of the linear stability region of the scheme.

Fig. 6 shows stability regions for the MUSTA-1 method for $c_z = 0$ and $c_z = 1/3$. The stability condition for the scheme can be approximately written as

$$c_x + c_y + c_z \leq 1.$$

Note that in the limiting case of $\lambda_2 = \lambda_3 = 0$ the scheme recovers the one-dimensional stability condition (35), which can be derived analytically.

In the rest of this section we carry numerical computations for multi-dimensional problems.

6.2 Computation of Double Mach Reflection

We solve the two-dimensional compressible Euler equations for an ideal gas in a rectangular domain. The formulation of the problem, computational setup and detailed discussion of the flow physics can be found in [31]. At the given output time a complicated flow pattern forms containing two Mach shocks, two slip surfaces and a jet. Figs. 7–8 show numerical results from the WENO scheme with the MUSTA flux of this paper on three meshes: 240×60, 480×120 and 960×240 cells. We observe that the scheme produces the flow pattern generally accepted in the present literature [31, 20] as correct, on all meshes. All discontinuities are well resolved and correctly positioned.

Delicate features of the flow, such as slip surfaces, are generally more difficult to resolve accurately, particularly when using symmetric methods or upwind methods with incomplete Riemann solvers. The results of the present MUSTA scheme are comparable to those with the *complete* HLLC Riemann solver [29] found in Figs. 2, 4 of [22], not reproduced here.

6.3 Three-Dimensional Explosion in Water

Finally, we solve the three-dimensional Euler equations for compressible liquids with the Tammann equation of state (48). The initial condition defined on $[-1:1] \times [-1:1] \times [-1:1]$ consists of two regions of constant but different values of liquid parameters separated by a sphere of radius 0.6:

$$(\rho, p) = \begin{cases} (1100,\ 5000), & r \leq 0.6 \\ (1000,\ 0.1), & r > 0.6 \end{cases}, \quad u = v = w = 0, \quad r^2 = x^2 + y^2 + z^2.$$

Here units are kg $\times$ m^{-3} and MPa for density and pressure, respectively. The constant values of γ and p_c in (48) are taken to be $\gamma = 7.15$ and $p_c = 300$ MPa, as in [10]. We compute the numerical solution at the output time 7×10^{-5}s on meshes of 51 and 101 cells in each coordinate direction. We use $C_{cfl} = 0.3$ for all runs. We compare the results of the WENO-MUSTA scheme with a reference radial solution, which is obtained by solving the one-dimensional Euler equations with a geometric source term on a very fine mesh. See Section 17.1 of [27] for details. The solution contains a spherical shock wave, a spherical contact surface, initially travelling away from the centre, and a spherical rarefaction wave travelling towards the origin $(0, 0, 0)$.

Figs. 9 – 10 show a comparison between the one-dimensional reference radial solution (solid line) and the cell averages of the three-dimensional WENO solution (symbols) along the radial

line that is coincident with the x-axis. We show the results only for $x > 0$. We present distributions of gas density ρ and pressure p. We observe that the MUSTA-WENO scheme obtains the correct solution, with the correct values behind the shock wave and the contact surface. As the mesh is refined, the numerical solution approaches the reference solution. The resolution of the smooth parts of the solution and of discontinuities is satisfactory, no spurious oscillations are present.

7 Summary and Conclusions

We have first presented a new upwind numerical flux, called GFORCE, that is a generalization of the FORCE symmetric flux. Then we have incorporated this flux into the MUSTA framework, leading to schemes of accuracy that is comparable to that of complete Riemann solvers for non-linear hyperbolic systems. But unlike conventional upwind methods with complete or incomplete Riemann solvers, our schemes are applicable to general systems of hyperbolic conservation laws. For a given vector of conserved variables, a corresponding flux vector and appropriate closure relations, the proposed MUSTA numerical flux is most easily computed. For multi-dimensional problems the unsplit versions of the schemes are linearly stable, unlike those of well-known symmetric fluxes such as Lax-Friedrichs and FORCE. The schemes have been implemented for the Euler equations in one, two and three space dimensions. Then the flux has been used as the building block for high order non-linear schemes via the TVD approach and the WENO approach. The performance of the new schemes has been demonstrated via the Euler equation for ideal gases, covolume gases and compressible water.

Acknowledgements. Part of the work was carried out while the first author was an EPSRC senior visiting fellow (Grant GR N09276) at the Isaac Newton Institute for Mathematical Sciences, University of Cambridge, UK, as joint organiser (with P. G. LeFloch and C. M. Dafermos) of the research programme on *Non-linear Hyperbolic Waves in Phase Dynamics and Astrophysics*, Cambridge, January to July 2003. The second author acknowledges the support provided by the Isaac Newton Institute, University of Cambridge, UK, as a participant to the same research programme.

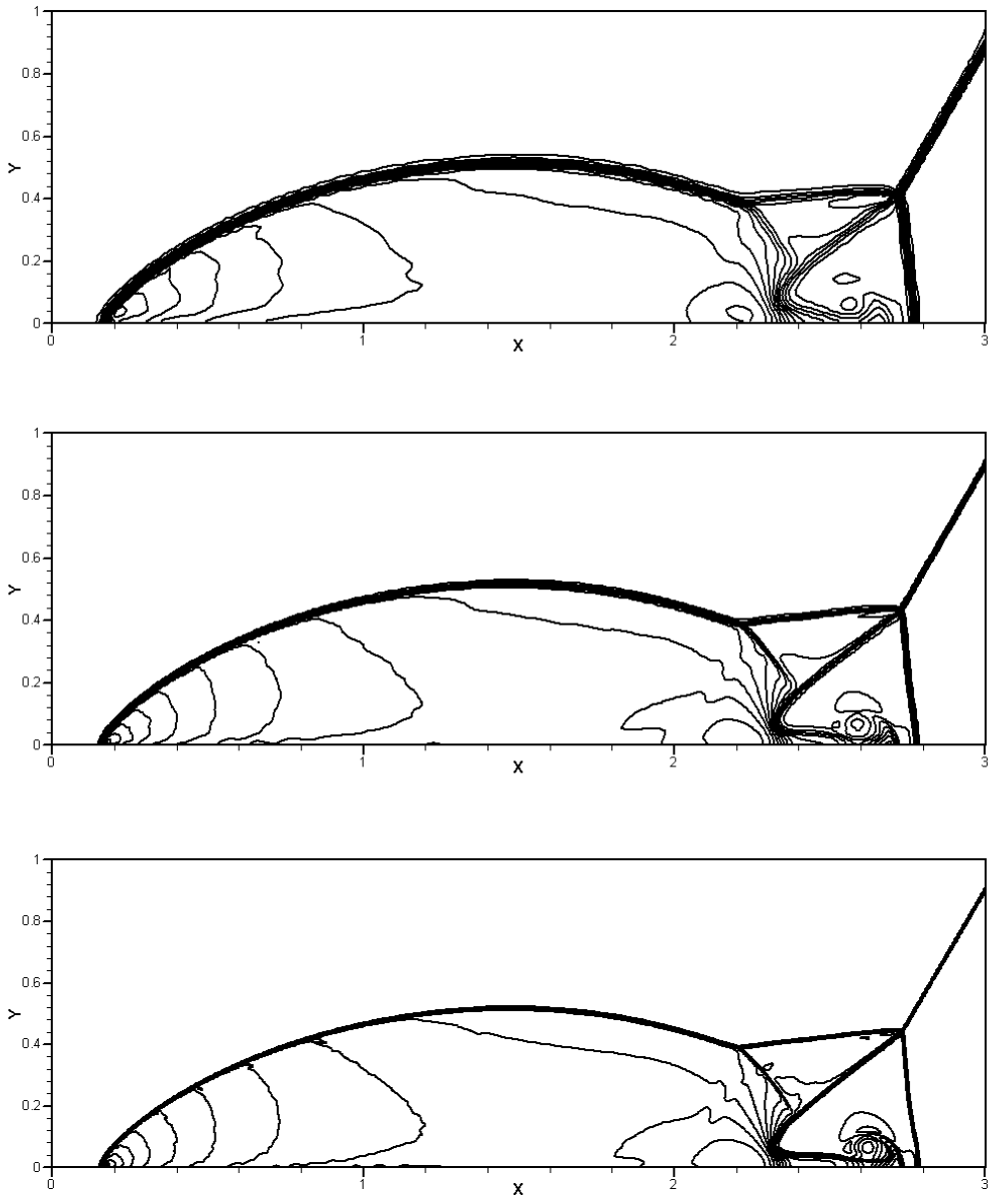

Figure 7: Double Mach reflection test problem. Results from the WENO-MUSTA scheme. Meshes of 240×60 (top), 480×120 (middle) and 960×240 (bottom) cells are used. 30 contour lines from 2 to 22.

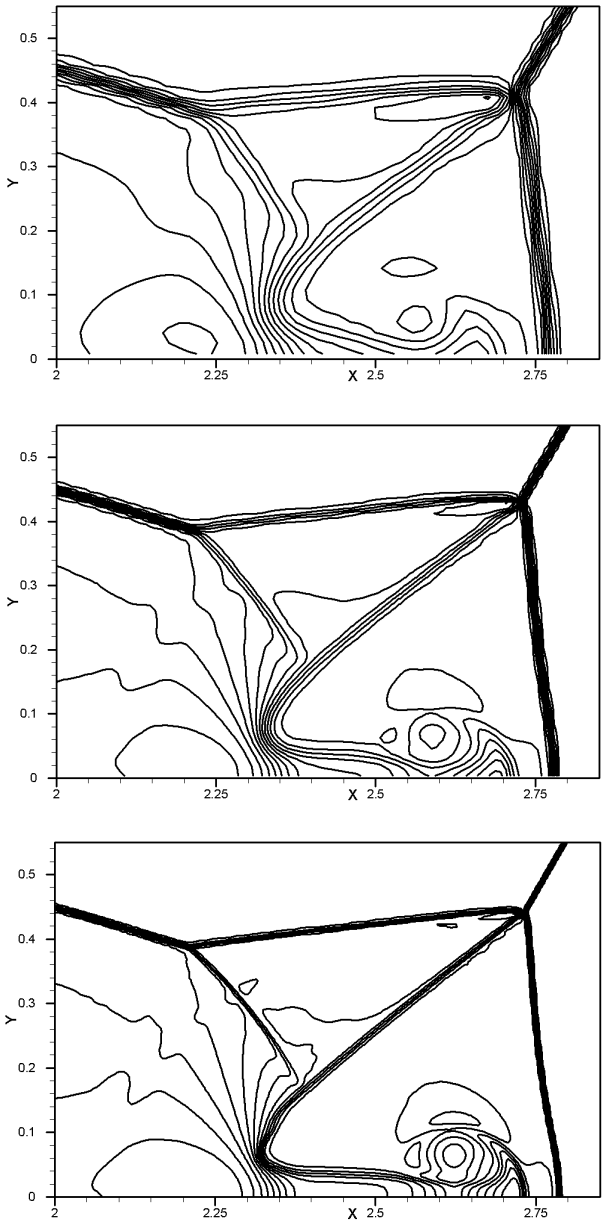

Figure 8: Double Mach reflection test problem. Results from the WENO-MUSTA scheme. Close-up view of Fig. 7 in the region around the contact surface.

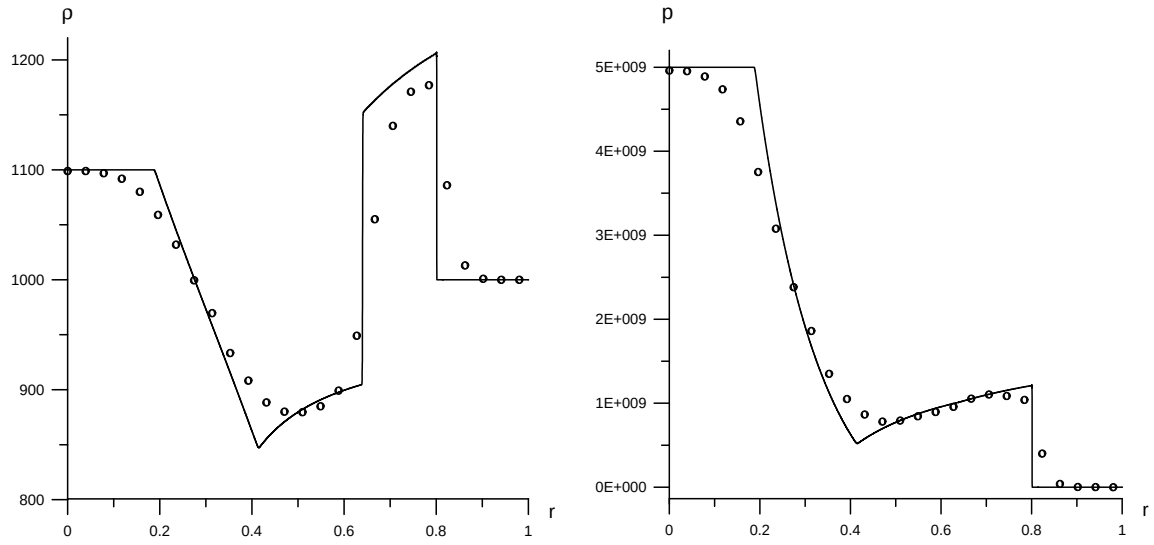

Figure 9: Spherical explosion in water. WENO-MUSTA 3D numerical (symbol) and reference radial (line) solutions for density (left) and pressure (right) for the mesh of $51 \times 51 \times 51$ cells.

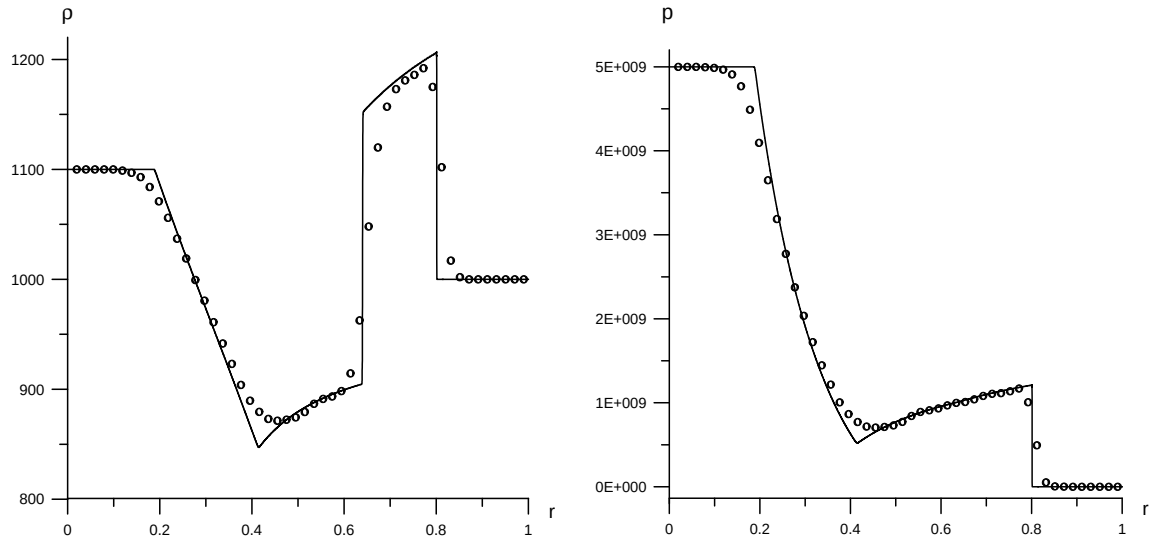

Figure 10: Spherical explosion in water. WENO-MUSTA 3D numerical (symbol) and reference radial (line) solutions for density (left) and pressure (right) for the mesh of $101 \times 101 \times 101$ cells.

References

[1] G. Q. Chen and E. F. Toro. Centred schemes for non-linear hyperbolic equations. *Journal of Hyperbolic Differential Equations*, 1(1):531–566, 2004.

[2] P. Colella and H. H. Glaz. Efficient Solution Algorithms for the Riemann Problem for Real Gases. *J. Comput. Phys.*, 59:264–289, 1985.

[3] R. Courant, E. Isaacson, and M. Rees. On the Solution of Nonlinear Hyperbolic Differential Equations by Finite Differences. *Comm. Pure. Appl. Math.*, 5:243–255, 1952.

[4] P. Glaister. An Approximate Linearised Riemann Solver for the Three–Dimensional Euler Equations for Real Gases Using Operator Splitting. *J. Comput. Phys.*, 77:361–383, 1988.

[5] J. Glimm. Solution in the Large for Nonlinear Hyperbolic Systems of Equations. *Comm. Pure. Appl. Math.*, 18:697–715, 1965.

[6] E. Godlewski and P. A. Raviart. *Numerical Approximation of Hyperbolic Systems of Conservation Laws*. Springer, 1996.

[7] S. K. Godunov. Finite Difference Methods for the Computation of Discontinuous Solutions of the Equations of Fluid Dynamics. *Mat. Sb.*, 47:271–306, 1959.

[8] S. K. Godunov, A. V. Zabrodin, and G. P. Prokopov. A Difference Scheme for Two-Dimensional Unsteady Aerodynamics. *J. Comp. Math. and Math. Phys. USSR*, 2(6):1020–1050, 1961.

[9] A. Harten, P. D. Lax, and B. van Leer. On Upstream Differencing and Godunov–Type Schemes for Hyperbolic Conservation Laws. *SIAM Review*, 25(1):35–61, 1983.

[10] M. J. Ivings, D. M. Causon, and E. F. Toro. On Riemann Solvers for Compressible Liquids. *Int. J. for Numer. Meth. in Fluids*, 28:395–418, 1998.

[11] C. B. Laney. *Computational Gasdynamics*. Cambridge University Press, 1998.

[12] P. D. Lax and B. Wendroff. Systems of Conservation Laws. *Comm. Pure Appl. Math.*, 13:217–237, 1960.

[13] D. Levy, G. Puppo, and G. Russo. A Fourth Order Central WENO Scheme for Multidimensional Hyperbolic Systems of Conservation Laws. *SIAM J. Sc. Comput.*, 24(2):480–506, 2002.

[14] E. H. Love and F. B. Pidduck. Lagrange's Ballistic Problem. *Phil. Trans. Roy. Soc. London*, 222:167–228, 1922.

[15] R. Menikoff and B. J. Plohr. The Riemann Problem for Fluid Flow of Real Materials. *Reviews of Modern Physics*, 61:75–130, 1989.

[16] Kolgan V. P. Application of the Principle of Minimum Derivatives to the Construction of Difference Schemes for Computing Discontinuous Solutions of Gas dynamics (in Russian). *Uch. Zap. TsaGI, Russia*, 3(6):68–77, 1972.

[17] L. Quartapelle, L. Castelletti, A. Guardone, and G. Quaranta. Solution of the Riemann Problem of Classical Gas Dynamics. *J. Comput. Phys.*, 190(1):118–140, 2003.

[18] P. L. Roe. Approximate Riemann Solvers, Parameter Vectors, and Difference Schemes. *J. Comput. Phys.*, 43:357–372, 1981.

[19] V. V. Rusanov. Calculation of Interaction of Non–Steady Shock Waves with Obstacles. *J. Comput. Math. Phys. USSR*, 1:267–279, 1961.

[20] C. Shi, J. Hu and C. W. Shu. A Technique for Treating Negative Weights in WENO Schemes. *J. Comput. Phys.*, 175(1):108–127, 2002.

[21] P. A. Thompson. *Compressible Fluid Dynamics.* McGraw–Hill, 1972.

[22] V. A. Titarev and E. F. Toro. Finite Volume WENO Schemes for Three-Dimensional Conservation Laws. *J. Comput. Phys.*, 201(1):238–260, 2004.

[23] E. F. Toro. Multi-Stage Predictor-Corrector Fluxes for Hyperbolic Equations. Technical Report NI03037-NPA, Isaac Newton Institute for Mathematical Sciences, University of Cambridge, UK, 17th June, 2003.

[24] E. F. Toro. A Fast Riemann Solver with Constant Covolume Applied to the Random Choice Method. *Int. J. Numer. Meth. Fluids*, 9:1145–1164, 1989.

[25] E. F. Toro. A Weighted Average Flux Method for Hyperbolic Conservation Laws. *Proc. Roy. Soc. London*, A423:401–418, 1989.

[26] E. F. Toro. On Glimm–Related Schemes for Conservation Laws. Technical Report MMU–9602, Department of Mathematics and Physics, Manchester Metropolitan University, UK, 1996.

[27] E. F. Toro. *Riemann Solvers and Numerical Methods for Fluid Dynamics, Second Edition.* Springer–Verlag, 1999.

[28] E. F. Toro and S. J. Billett. Centred TVD Schemes for Hyperbolic Conservation Laws. *IMA J. Numerical Analysis*, 20:47–79, 2000.

[29] E. F. Toro, M. Spruce, and W. Speares. Restoration of the Contact Surface in the HLL–Riemann Solver. *Shock Waves*, 4:25–34, 1994.

[30] B. van Leer. Towards the Ultimate Conservative Difference Scheme I. The Quest for Monotonicity. *Lecture Notes in Physics*, 18:163–168, 1973.

[31] P. Woodward and P. Colella. The Numerical Simulation of Two–Dimensional Fluid Flow with Strong Shocks. *J. Comput. Phys.*, 54:115–173, 1984.